Proceedings of the ASME 2020 Fluids Engineering Division Summer Meeting
FEDSM2020
July 13-15, 2020, Virtual, Online
FEDSM2020-20338

RANS VOF SIMULATIONS OF DENSITY-STRATIFIED AIR-WATER FLOW IN A 2D CHANNEL

Chandrima Jana Maiti
Dept. of Mechanical & Materials Engineering
University of Cincinnati
Cincinnati, Ohio 45221 USA
janaca@mail.uc.edu

Urmila Ghia
Dept. of Mechanical & Materials Engineering
University of Cincinnati
Cincinnati, Ohio 45221 USA
ghiau@ucmail.uc.edu

Leonid A. Turkevich
National Institute for Occupational Safety and Health
Centers for Disease Control and Prevention
Cincinnati, Ohio 45226 USA
llt0@cdc.gov

Abstract

We perform RANS-VOF simulation of density-stratified, fully developed air-water flow in a 2D channel. The flow is completely specified by the (common) driving pressure gradient down the channel and by the fill factor (relative height of the heavier phase to the total height of the channel). Varying the pressure gradient and fill factor results in different flow combinations: namely, laminar air/laminar water, turbulent air/laminar water, turbulent air/turbulent water, laminar air/turbulent water. The focus of the study is the near-interface interaction when either or both phases are turbulent. The RANS-VOF equations are solved on a 2D channel with periodic inlet/outlet boundary conditions. For a fixed fill factor, the Reynolds numbers of each phase varies monotonically with driving pressure gradient. However, at fixed pressure gradient, the fluid Reynolds numbers are non-monotonic at high fill factor. This Reynolds number phase diagram is important in understanding the laminar and turbulent regimes of each phase. The mean velocity is axial (down the channel) and exhibits a dip below the free surface whenever one of the phases is turbulent. As expected, the diagonal Reynolds stresses <u'u'>, <v'v'>, are strongly coupled between the phases, however coupling in <u'v'> is less pronounced.

1. Introduction

Stratified flow is a basic flow pattern for gas-liquid two-phase flows in a gravitational field, where the lighter fluid flows above the heavier one. The stratified flow regime is frequently encountered in long distance pipeline networks (e.g. steam and water, natural gas and oil), power plants, in river and culvert flow. Stratified flow through ducts is characterized by a mixed-boundary corner formed by the intersection of the vertical side wall and the horizontal free surface. An important feature of the mixed-boundary corner is the interaction between wall-turbulence and the air-water interface. At a wall boundary, all velocity components vanish, resulting in a region of high shear. By contrast, an air-water interface cannot support mean shear. The mixed-boundary corner conflates the different behaviors of turbulence in these fundamentally different boundaries, and the complexities that arise affect the transport of mass and momentum [1, 2, 3, 4]. As a precursor to the full 3D

stratified flow problem, we first study the stratified flow through a 2D flow domain, i.e., without the side walls. The 2D flow still permits investigation of the behavior of the turbulence across the fluid interface. Previous studies on the 3D problem have frequently treated the interface as a non-deforming free slip boundary [1-3, 5]. Such a treatment, while retaining the coupling of the two fluids via their mean flow (a common interface velocity and continuity of the shear stress at the interface), neglects any coupling via the turbulent Reynolds stresses. In such a treatment, the 'solid' free surface acts as a source of turbulent stresses and artificially supports a boundary layer; turbulence is not allowed to communicate between the fluid phases. In the present work we study the propagation of turbulence across an actual air-water interface.

2. Geometry

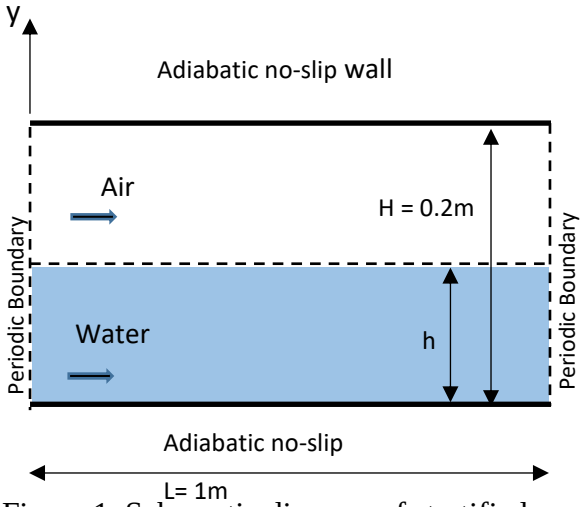

Figure 1. Schematic diagram of stratified air-water flow domain

Figure 1 shows the geometry of the solution domain, which is a 2D channel bounded by adiabatic no-slip walls. The total length of the domain is L=1m, and height H=0.2m. The level of water in the domain is specified by h. Fill factor, f, is the ratio of the level of water to the total height of the domain, i.e., f = h/H. It describes how full the domain is with the heavier fluid.

2.1 Computational details

We perform RANS-VOF simulations of density-stratified, fully developed air-water flow in a 2D channel, using the finite volume approach available with the commercial CFD package Ansys Fluent 15.0. The discretized equation, along with the initial and boundary conditions, were solved using the segregated solution method to obtain the numerical results. The mass and momentum conservation equations were solved iteratively, and a pressure-correction equation was used to ensure conservation of mass and momentum. The Reynolds stress model (RSM) was used to treat turbulence phenomena in both phases. The grids are structured, cartesian, algebraically refined both at the walls and interface (the most refined grid consists of $5x10^4$ cells).

2.2 Interface capturing: Volume of fluid (VOF) method

The volume of fluid (VOF) method, which is a surface-capturing technique applied to a fixed Eulerian grid, is used for interface modeling. This model is based on the concept of a phasic volume fraction (denoted here by α, the volume fraction of water in a cell) [6]. An intermediate value $0 < \alpha < 1$ within a discrete mesh cell represents a segment of interfacial region of two fluids:

- $\alpha = 0$: the cell is empty of water
- $\alpha = 1$: the cell is full of water
- $0 < \alpha < 1$: the cell contains the air-water interface

To compute the time evolution of the interface, we need to move the volume fractions through a grid in a way such that the step function nature of the volume fraction is maintained.

The kinematic equation for the water volume fraction is a continuity equation:

$$\frac{1}{\rho_q}\left[\frac{\partial}{\partial t}(\alpha\rho) + \nabla.(\alpha\rho\vec{v})\right] = 0 \qquad (1)$$

which is solved for the heavier fluid (the secondary fluid). The volume fraction of the lighter fluid (primary fluid) is given by 1 – α.

The properties appearing in the transport equation such as density, are determined by a volume fraction average of all fluids in the cell, $\rho = \rho_w \alpha + \rho_a (1-\alpha)$.

These properties are then used to solve a single momentum equation through the domain, and the computed velocity field is shared among the fluids. The VOF equation is solved using the implicit scheme. To calculate the convection and diffusion fluxes through the control volume faces, the compressive scheme is used, which is a second order reconstruction scheme based on a slope limiter.

2.3 Governing equations

The governing equations describing the incompressible viscous flow of two immiscible fluids are

The mass conservation equation:

$$\nabla.(\vec{v}) = 0 \qquad (2)$$

The RANS equation:

$$U_j\frac{\partial U_i}{\partial x_j} + \frac{1}{\rho}\frac{\partial p}{\partial x} = \frac{1}{\rho}\frac{\partial}{\partial x_j}(\bar{\tau}_{ij} + \lambda_{ij}) \qquad (3)$$

where $\bar{\tau}_{ij}$ is the fluid stress tensor, λ_{ij} is the Reynolds stress tensor given by

$$\bar{\tau}_{ij} = -\ \rho\overline{u_i' u_j'} \qquad (4)$$

The momentum equation is dependent on the volume fractions of all the phases through the properties ρ and μ.

2.4 Turbulence model

Reynolds stress model (RSM) is used to study the turbulence phenomena. The RSM closes the RANS equations by solving a transport equation for the Reynolds stresses ($\rho\overline{u_i' u_j'}$) appearing in the momentum equations, together with an equation for the dissipation rate.

The flow is driven by a common pressure gradient, which is the input for the numerical simulation. A series of simulations have been carried out varying both the pressure gradient and the fill factor to obtain cases where either or both phases are turbulent.

3. Grid-dependence study

To evaluate the impact of grid resolution on the simulated results, all the cases were simulated on three successively finer grids (successively refined by a factor of 1.5 in each direction). The discretization error was estimated (Grid Convergence Index (GCI), Celik et al. [7]) for the half-filled case, driven by dp/dx = -0.095 Pa/m. The parameters used for this estimation are i) u_{max} in the water domain below the interface; (GCI=0.0145%) ii) computed mass flow rates resulting in the corresponding Re: Re_{air} (GCI=8.31%), Re_{water} (GCI=0.066%).

4. Results and discussion

The Reynolds number phase diagram (Figure 2) describes mass flow in each phase at a given fill factor and pressure drop.

Laminar and turbulent phases are demarcated qualitatively by dashed lines at Re ~ 2000. Solid lines connect simulations conducted at the same fill factor. Lower (common) driving pressure gradients correspond to points closer to the $Re_w = Re_a = 0$ corner (lower left).

At a fixed fill factor, the Reynolds number of each phase varies monotonically with the driving pressure gradient. However, at fixed pressure gradient, the fluid Reynolds numbers are non-monotonic at high fill factor. For more general geometries, such a Reynolds number phase diagram establishes a relation between pressure drive, fill factor and flow rates of each phase.

Axial velocity profile

Representative average velocity profiles for the four flow scenarios namely: laminar air/ laminar water, turbulent air/laminar water, turbulent air/turbulent water, and, laminar air/turbulent water is shown in Figure 3. When both phases are laminar, we obtain the classic parabolic velocity profile for air and half parabola for water.

The near-parabola air velocity profile indicates that water provides larger resistance to the air flow, and hence it acts like a 'wall'. In the other three cases, where either or both phases are turbulent, the maximum velocity in the heavier phase occurs approximately 5% below the free surface. There is thus a 'velocity dip' at the free surface; this is absent in the free shear lid model of the interface. The low Reynolds number mean velocity profiles are also flatter than the corresponding laminar profiles, again, whenever the other phase is turbulent. Thus the laminar to turbulent transition appears to occur at a lower Reynolds number (than in single phase flow) if the other phase is already turbulent.

Reynolds stresses

Figure 4 displays the diagonal axial Reynolds stress <u'u'> through the two phases: a), d) turbulent air/laminar water (f = 0.25); b), e) turbulent air/turbulent water (f = 0.5); c), f) laminar air/turbulent water (f = 0.75) – the panels at left display the global behavior, the panels at right focus on the behavior at the interface.

We first discuss the case of turbulent air/laminar water (fig. 4a). The solid wall at the top of the channel serves as a strong source of turbulent fluctuations (well-defined peak 1). In our RANS VOF simulation, the air-water interface generates turbulent fluctuations in the air (peak 2). While broader than the <u'u'> peak 1 from the top solid surface, the amplitude of the peak 2 in <u'u'> turbulence fluctuations from the free surface closely tracks that from the solid surface, qualitatively reflecting the fact that the less-mobile water phase generates shear at the interface on the moving air phase. Unlike the moving lid model (where there are no turbulent fluctuations in the water subphase), turbulence fluctuations penetrate into the laminar water subphase and decay with increasing depth; note the significantly smaller value (down by a factor of 10^{-2}) of these fluctuations on the water side of the interface. It is characteristic of all the cases that the ratio of fluctuations at the interface between water and air phases is ~ 10^{-2}. Fluctuations on the air side of the interface are reduced (fig. 4d).

The behavior of the axial turbulent fluctuations for the case of turbulent air/turbulent water (fig. 4b) is very similar. Again, there is a sharp peak1 in turbulent fluctuations at the top solid wall. The air-water interface is a more efficient source of

axial fluctuations (peak 2); again, the strength of these two peaks tracks each other with pressure gradient. Again, the turbulent axial fluctuations penetrate into the water subphase (peak 3) with a relative strength of $\sim 10^{-2}$; while it is not surprising for turbulent fluctuations <u'u'> to be present in the turbulent water phase, the free surface does not act as a solid wall source of such fluctuations, but rather the turbulent fluctuations 'leak' across the interface. The bottom solid surface predictably acts as a weak source of such fluctuations (peak very small on this scale). Fluctuations on the air side of the interface are reduced (Fig. 4e).

The behavior of the axial turbulent fluctuations is counter-intuitive for the case of laminar air/turbulent water (fig. 4c). The bottom solid wall predictably acts as a weak source of axial fluctuations, but, again, this is small on the scale of fig. 4c. Surprisingly, the nominally laminar air exhibits axial turbulent fluctuations, generated both at the free surface (larger amplitude peak 2) and at the solid top surface (smaller amplitude peak 1); the ratio of axial fluctuations between water and air remains $\sim 10^{-2}$, but in this case the fluctuations are 'amplified' in the nominally laminar air. The ability of the top solid surface to generate a boundary layer with concomitant axial fluctuations is the result of the spatial extent of turbulent fluctuations leaking through into the nominally laminar super-phase. Fluctuations on the water side of the interface are amplified (fig. 4f).

Figures 5 display the diagonal vertical Reynolds stress <v'v'> through the two phases: a), d) turbulent air/laminar water (f = 0.25); b), e) turbulent air/turbulent water (f = 0.5); c), f) laminar air/turbulent water (f = 0.75). For the turbulent air cases (figs. 5a, 5b), the magnitude of <v'v'> is about half that of the axial stress <u'u'>; for the laminar air case (fig. 5c), the magnitude is about one quarter that of the axial stress. The vertical fluctuations necessarily vanish at both top and bottom solid surfaces. The vertical fluctuations are maximal just above the free surface for all cases, and, in all cases, there is significant penetration into the water sub phase. Again, vertical water fluctuations are amplified near the free surface for the laminar air/turbulent water case (fig. 5f). Both features are suppressed in the moving lid approximation.

Figures 6 display the off-diagonal Reynolds shear stress <u'v'> through the two phases: a), d) turbulent air/laminar water (f = 0.25); b), e) turbulent air/turbulent water (f = 0.5); c), f) laminar air/turbulent water (f = 0.75). The structure of the off-diagonal stress is qualitatively similar for all three cases, although the magnitude for the laminar air case (fig. 6c) is significantly smaller than that for the turbulent air cases—note that this latter would vanish for the moving lid model. For all cases, the magnitudes of <u'v'> are comparable to the magnitudes of <v'v'>. Again, the behavior of <u'v'> near the interface parallels that of the diagonal stresses.

5. Conclusions

RANS-VOF simulations have been performed of density-stratified, fully-developed air-water flow in a 2D channel. Varying the pressure gradient (that drives the flow) and the fill factor enables simulations to be performed in all regimes, namely where each of the phases is either laminar or turbulent. The rich fluctuation behavior at the interface is examined in detail—such fluctuations are suppressed in the usual moving lid treatment of the free surface.

It is expected that a similar approach can be used to treat the mixed boundary behavior of a wall-bounded free surface in 3D channel flow.

Disclaimer

The findings and conclusion in this paper are those of the authors and do not necessarily represent the views of the National Institute for Occupational Safety and Health. Mention of any product or company name does not constitute endorsement by the Center of Disease Control and Prevention. None of the authors has a financial relation with a commercial entity that has an interest in the subject of this manuscript. This material is declared a work of the US government and is not subject to copyright protection in the United States.

References

[1] Broglia, R., Pascarelli, A., and Piomelli, U., 2003, "Large-Eddy Simulations of Ducts with a Free Surface," J. Fluid Mech., **484**(484), pp. 223–253.

[2] Joung, Y., and Choi, S.-U., 2010, "Direct Numerical Simulation of Low Reynolds Number Flows in an Open-Channel with Sidewalls," Int. J. Numer. Methods Fluids, **62**(8), pp. 854–874.

[3] Grega, L. M., Hsu, T. Y., and Wei, T., 2002, "Vorticity Transport in a Corner Formed by a Solid Wall and a Free Surface," J. Fluid Mech., **465**, pp. 331–352.

[4] Lee, J., Suh, J., and Sung, H. J., 2011, "Direct Numerical Simulation of Turbulent Open Channel Flow with Froude Number Effect," 7th Int. Symp. Turbul. Shear Flow Phenom.

[5] Shi, J., Thomas, T. G., and Williams, J. J. R., 1999, "Large-Eddy Simulation of Flow in a Rectangular Open Channel," J. Hydraul. Res., **37**(3), pp. 345–361.

[6] Hirt, C. W., 1981, "Volume of Fluid (VOF) Method for the Dynamics of Free Boundaries *," **225**, pp. 201–225.

[7] Celik, I.B., Ghia, U., Roache, P.J., Freitas, C.J., Coleman, H., Raad, P.E., J.F.E., 2008, "Procedure for Estimation and Reporting of Uncertainty Due to Discretization in CFD Applications," **130**(July), pp. 1–4.

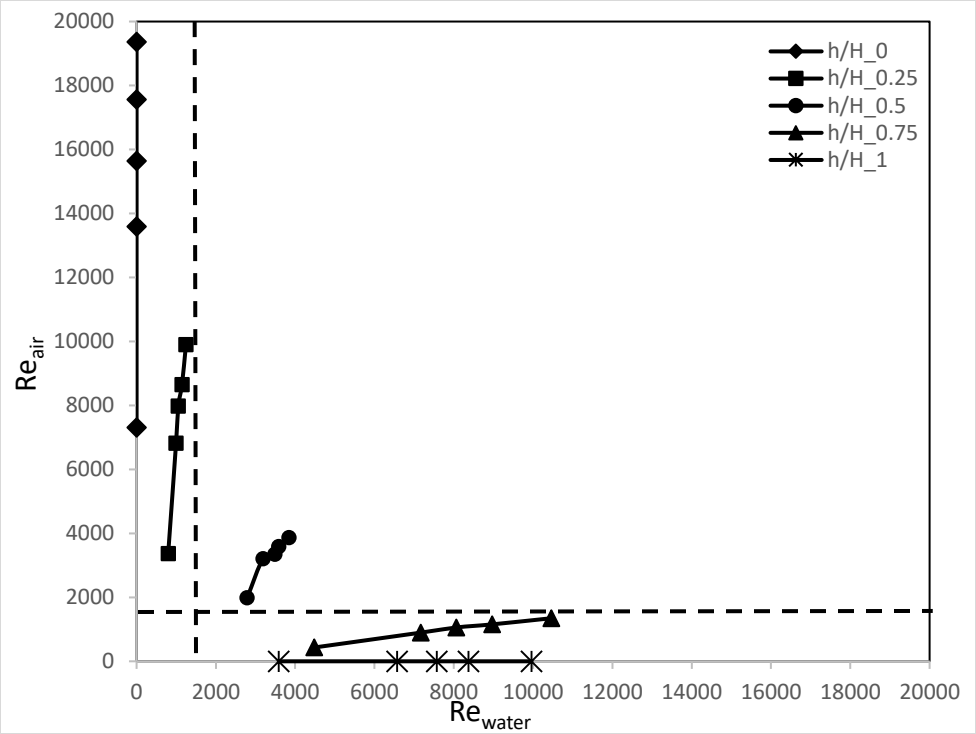

Figure 2. Graphical representation of computed phasic mass flow rates driven by a common pressure gradient at different fill factors

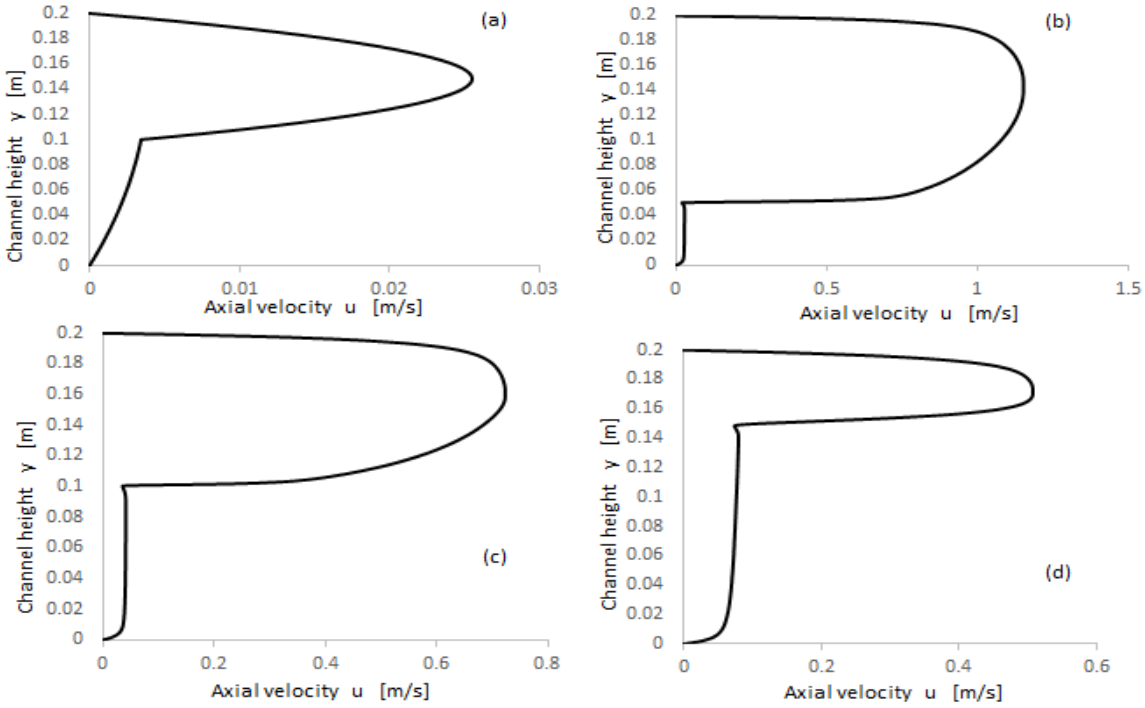

Figure 3. Representative axial velocity profiles (a) Laminar-Laminar (b) Turbulent-Laminar (c) Turbulent-Turbulent (d) Laminar-Turbulent

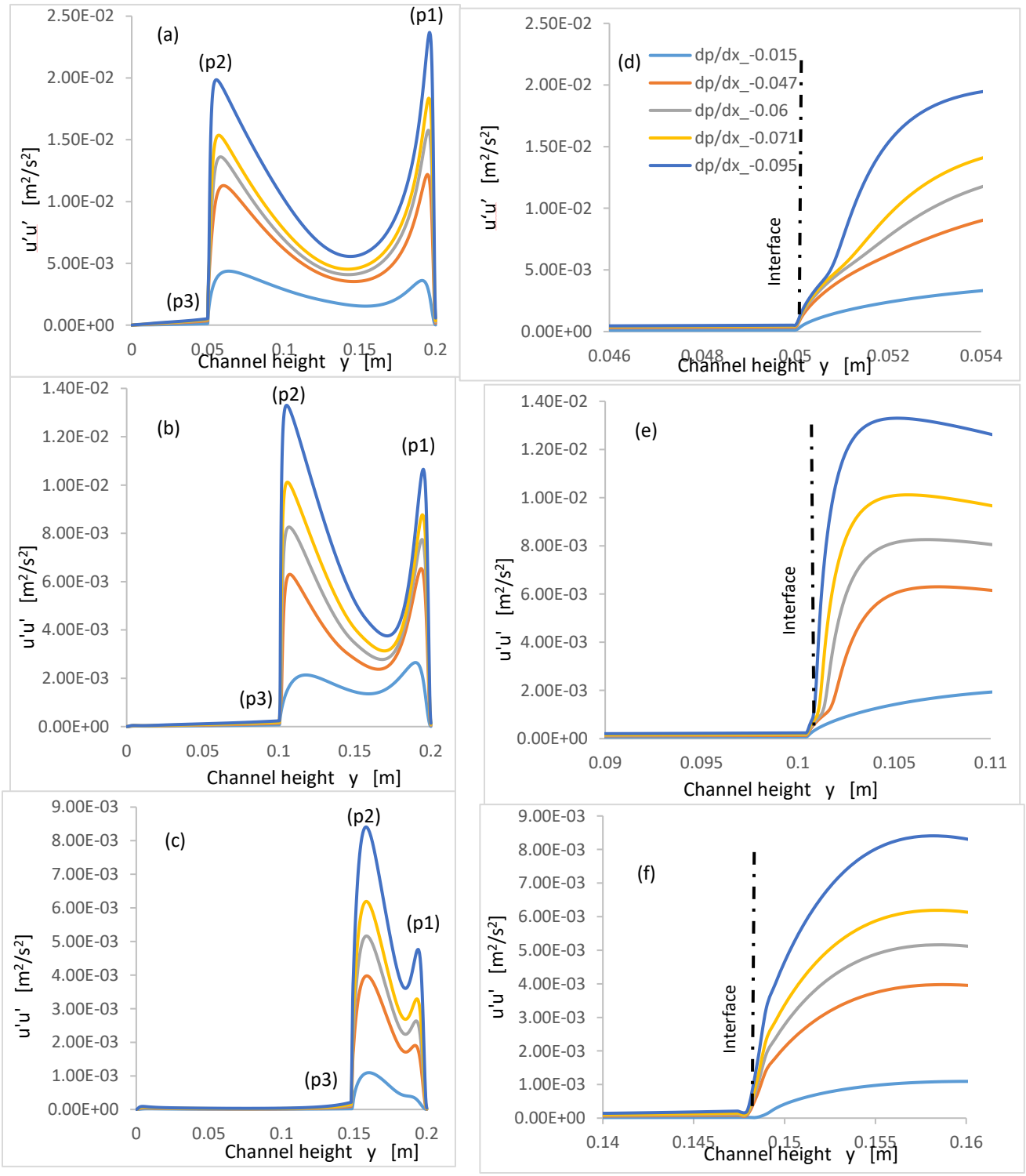

Figure 4. Reynolds stress <u'u'> profiles (global and near-interface): a), d) f = 0.25; b), e) f = 0.5; c), f) f = 0.75

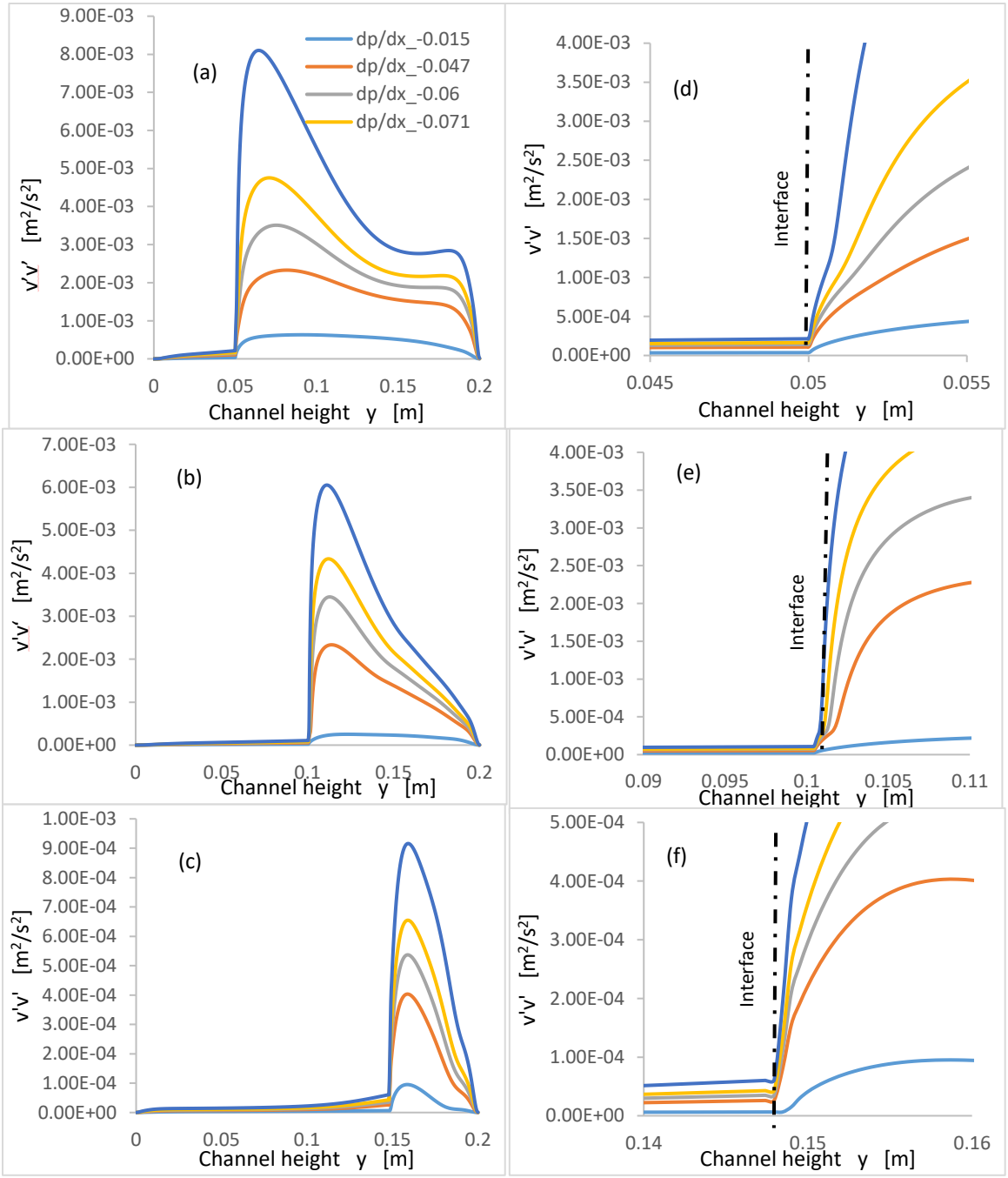

Figure 5. Reynolds stress <v'v'> profiles (global and near-interface): a), d) f = 0.25; b), e) f = 0.5; c), d) f = 0.75

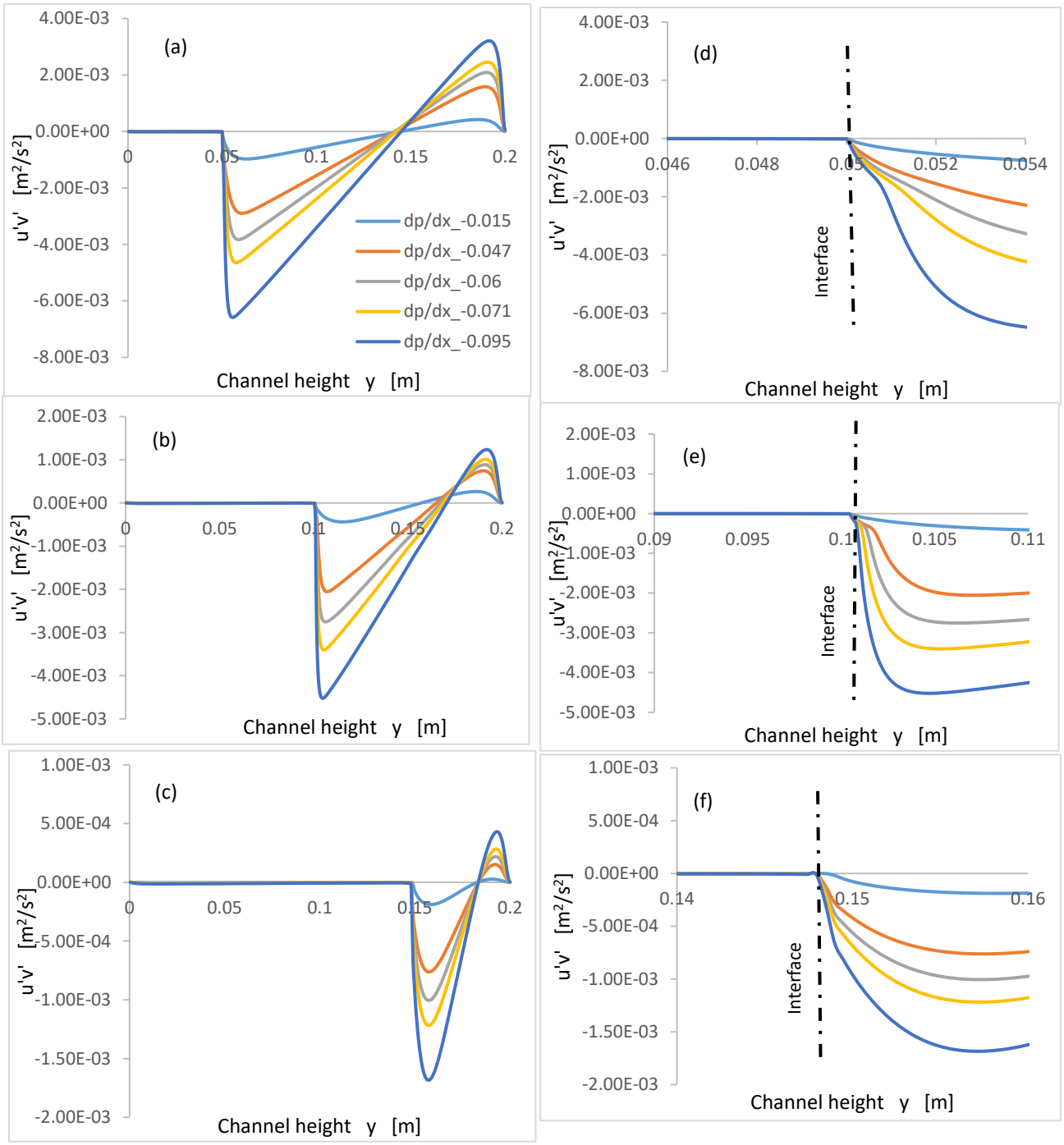

Figure 6 Reynolds shear stress <u'v'> profiles (global and near-interface): a), d) f = 0.25; b), e) f = 0.5; c), f) f = 0.75